

Electronic properties and bonding sites for chlorine chemisorption on Si(111)-(7×7)

R. D. Schnell, D. Rieger, A. Bogen, F. J. Himpsel,* K. Wandelt† and W. Steinmann
Sektion Physik der Universität München, D-8000 München 40, Federal Republic of Germany

(Received 16 July 1985)

The adsorption of chlorine on Si(111)-(7×7) has been studied with various photoemission techniques with the use of synchrotron radiation. At room temperature, bonding of one, two, and three chlorine atoms to a Si surface atom was observed with Si 2*p* core-level shifts of 930, 1830, and 2730 meV to higher binding energy, respectively. After annealing to 400°C only monochloride species remained. For the annealed (400°C) ordered Cl/Si(111)-(7×7) system four chlorine-induced valence states could be distinguished with polarization-dependent angle-resolved photoelectron spectroscopy, i.e., two nondispersive bonding Cl-Si states: σ ($E_B=7.21$ eV below the top of the valence band), s ($E_B=8.7$ eV), and two dispersing Cl-Cl π states of different symmetry $\pi^+\pi^-$. The dispersion of the π^+ (π^-) band is $\Delta E^+=1000$ meV ($\Delta E^-=320$ meV) along $\Gamma\bar{M}$ and $\Delta E^+=900$ meV ($\Delta E^-=450$ meV) along $\Gamma\bar{K}$. The photoemission angular distribution of the σ and s states shows maximum intensity in the gaps of the projected Si band structure and attenuated emission where the chlorine bands overlap with Si bands. The attenuation is explained by hybridization with the substrate bands.

I. INTRODUCTION

The interaction of chlorine with silicon surfaces is of interest both in pure and applied physics. Chlorine is known to form stable chemisorbed layers on various semiconductor surfaces at room temperature.¹⁻³ In contrast with many other adsorbates one has well-ordered overlayers on semiconductor surfaces. Especially the chemisorption on Si(111) has been the subject of various experimental²⁻¹¹ and theoretical^{5-7,12-20} investigations and has become a prototype system for studying the interaction of adsorbates with semiconductor surfaces. The adsorption is the first step of the reaction of chlorine with solid silicon and is also of importance for the interpretation of the reaction processes that occur during plasma etching²¹ and chemical vapor deposition.

For a description of the chemisorption system the atomic arrangement and the electronic structure at the surface have to be known. After adsorption on the Si(111)-(2×1) cleavage face, chlorine forms an ordered (1×1) overlayer that has been studied with polarization-dependent^{2,5} and with angle-resolved photoelectron spectroscopy.⁷ On this surface the chlorine atoms adsorb on top of the silicon surface atoms and saturate their single broken bonds. A comparison of polarization-dependent photoelectron spectra² of chlorine chemisorbed at room temperature on both the thermodynamically stable Si(111)-(7×7) surface and the cleaved Si(111)-(2×1) surface showed pronounced differences.

As yet, a detailed study with angle-resolved photoelectron spectroscopy is not available for Cl/Si(111)-(7×7). Surface extended x-ray-absorption-fine-structure (SEXAFS) measurements, however, found chlorine on top of the silicon surface atoms on this surface as well after annealing at about 400°C.¹¹

We have investigated the chlorine adsorption on

Si(111)-(7×7) with various photoemission techniques using synchrotron radiation in order to determine the bonding geometry and the electronic structure after room temperature adsorption and annealing. We find the following new results: With surface-sensitive core-level photoelectron spectroscopy we are able to distinguish three different bonding geometries at room temperature. After annealing the chlorine atoms are found only in the on-top configuration on Si surface atoms. The symmetry and the dispersion of the chlorine-induced valence bands of this ordered chemisorbed layer have been determined with polarization-dependent angle-resolved photoelectron spectroscopy. Two bonding Cl-Si states were observed and a two-dimensional Cl 3*p*-like band. A splitting of this band into states of even and odd mirror symmetry could be distinguished by applying dipole selection rules. The angular intensity distribution of photoemission of the two bonding Cl-Si states gives information about their localization in momentum space. The photoemission intensity is strongest where these states fall into gaps of the projected band structure and thus cannot hybridize with the substrate bands.

II. EXPERIMENTAL

The experiments were carried out at the dedicated storage ring BESSY [Berliner Elektronenspeicherring-Gesellschaft für Synchrotronstrahlung (Berlin, Germany)]. The synchrotron radiation was dispersed by the toroidal-grating monochromator TGM 3.²² The photoemission experiments were performed with an ellipsoidal-mirror display analyzer (EMDA).^{23,24} Figure 1(a) shows a schematic drawing of the analyzer. It consists of an ellipsoidal-mirror low-pass energy filter and a spherical-grid high-pass energy filter with angular resolving capability within the whole acceptance cone of the analyzer

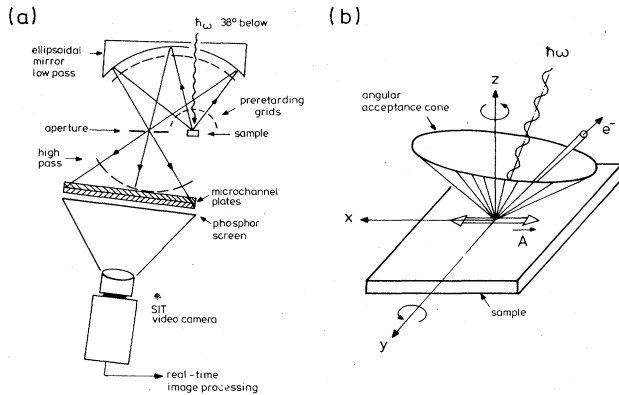


FIG. 1. (a) Schematic drawing of the ellipsoidal-mirror display analyzer (EMDA). (b) Sample geometry showing the angular acceptance cone (90°) of the EMDA for a configuration with *s*-polarized light incident on the sample.

[see Fig. 1(b)]. The flexibility of the analyzer provides different modes of operation:²⁴ (1) The two-dimensional angular intensity distribution of the photoelectrons $N(\theta, \phi)$ for a distinct kinetic energy is visualized on the phosphor screen behind the microchannel plates and monitored by a precision silicon-intensified-target (SIT) video camera. (2) Angle-resolved photoelectron spectra $N(E, \theta, \phi)$ are measured by recording angular distribution pictures for different kinetic energies. A real-time image-processing system is used for digital video data processing. This enables us to measure photoelectron spectra within the whole angular acceptance cone simultaneously for all angles. Measuring times are typically 30–90 min in this mode of operation. For typical spectra, see Fig. 5. (3) Angle-integrated photoelectron spectra $N(E)$ are measured with standard pulse-counting electronics connected to the phosphor screen. The overall energy resolution (monochromator + analyzer) was typically 300 (400) meV for the valence band (core-level) spectra presented in this paper. In the angle-resolved mode the angular resolution is $\pm 1.5^\circ$. All sample preparations were carried out in a separate preparation chamber connected to the spectrometer via a straight through valve. Cleaning of the Si(111) surfaces was performed by repeated cycles of mild sputtering (600–800-eV Ar^+) and heating ($\sim 1000^\circ\text{C}$). Nearly intrinsic wafers were used ($\sim 10 \Omega \text{ cm}$, *n*-type, phosphor doped) to minimize band-bending effects within the escape depth of the photoelectrons. For the adsorption experiments the crystals were exposed to a beam of chlorine emerging from an AgCl solid-state electrochemical cell²⁵ until saturation coverage was achieved. This source avoids exposing the whole chamber to the highly reactive Cl_2 gas. After chlorine adsorption, a low-energy electron diffraction (LEED) pattern is seen which consist of six-pointed stars of fractional-order spots around each integer-order spot.

III. RESULTS AND DISCUSSION

A. Surface core-level shifts

Core-level shifts of surface atoms can give information about the local bonding configuration of adsorbates.²⁶ In particular, several coexisting bond geometries with different oxidation states of surface atoms^{27,28} can be detected. For example, with GaAs (110) we recently observed pronounced shifts of the As $3d$ core level after adsorption of chlorine, while the Ga $3d$ level remained unaffected, suggesting bonding of the chlorine atoms exclusively to As surface atoms.²⁵ Figure 2 shows the results for $\text{Cl}/\text{Si}(111)-(7 \times 7)$. The surface-sensitive core-level spectrum after saturated room-temperature adsorption is shown in Fig. 2(a). Annealing the surface to about 400°C for 5 min produces the spectrum of Fig. 2(b). To point out the differences between the two spectra more clearly all the Si $2p^{1/2}$ contribution and the secondary-electron background have been subtracted. The results of this decomposition are shown in Figs. 2(c) and 2(d). For the Si $2p^{1/2}$ subtraction it is only necessary to know the spin-orbit splitting of 0.61 eV and the Si $2p^{1/2}$ –to–Si $2p^{3/2}$ intensity ratio of 0.54.

After room-temperature adsorption, three shifted core-level contributions of the surface (1^+ , 2^+ , 3^+) are seen beside the main bulk line. The binding-energy shifts and the relative intensities of the contributions used to fit the ex-

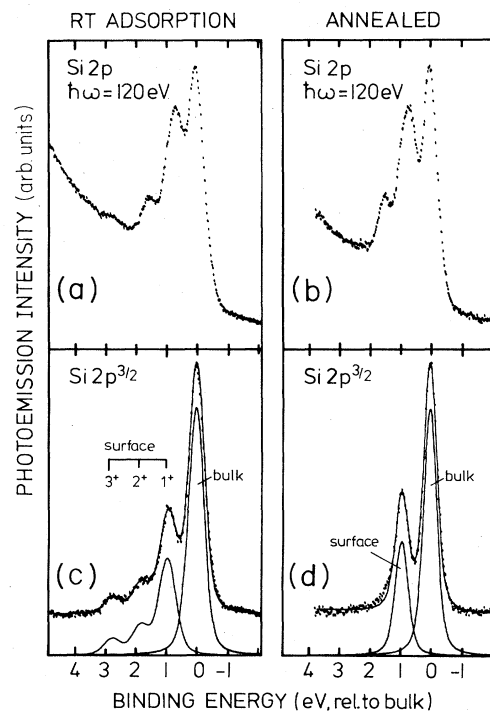


FIG. 2. Si $2p$ core-level photoelectron spectra for saturated chlorine adsorption at (a) room temperature, (b) after annealing this surface to about 400°C , and (c) and (d) the same spectra after subtraction of the Si $2p^{1/2}$ contribution and the background.

perimental curve are listed in Table I. We assign these surface components to binding of silicon surface atoms to either one (1^+), two (2^+), or three (3^+) chlorine atoms. Similar results with bonding to various numbers of adsorbate atoms and nearly linear surface core-level shifts induced by charge transfer have been observed for fluorine and oxygen on silicon surfaces.^{27,28} The chlorine atoms cannot penetrate the surface. The potential barrier for penetration is too high.¹⁹ This explains the saturation behavior during adsorption. In contrast, fluorine atoms are able to penetrate the surface, break silicon-silicon bonds, and etch the surface even at room temperature.^{29,30} Etching with chlorine is only observed in combination with rare-gas ions³¹ or laser light³² incident on the surface. On the ideal Si(111) surface, bonding of more than one chlorine atom to a silicon surface atom is not possible because the chlorine radius is too large and a surface atom has only one unsaturated dangling bond. But the clean Si(111)-(7×7) surface is known from scanning-tunneling microscopy³³ to have microscopic protrusions and cavities within the (7×7) real-space unit mesh. At these places bonding of silicon to two or three chlorine atoms is conceivable using various structural model.³⁴ After saturation adsorption of chlorine at room temperature the LEED pattern is modified to the so-called “(7×1)” pattern^{35,36} which is also observed after hydrogen adsorption. This LEED pattern can be produced by triangular islands of locally ideal (1×1) structure separated by troughs which are also present at the clean (7×7) surface. The islands should have approximately the area of half the (7×7) real-space unit mesh. After annealing, the fractional-order spots are sharpened. The effect on the Si 2*p* core-level spectrum is seen in Fig. 2(d). The 2^+ and 3^+ components of the surface signal have vanished and the 1^+ component has at the same time increased in intensity. However, the increase in the 1^+ intensity does not make up for the loss in 2^+ and 3^+ intensity (see Table I). For the fit in Fig. 2(c) the surface contributions had to be broadened relative to the bulk line. After annealing both the bulk and surface 1^+ components are fitted with the same linewidth: an intrinsic Lorentzian width of 200 meV (Ref. 37) and an extra Gaussian width of 400 meV for the instrumental broadening. Thus annealing causes a rearrangement and ordering of the chemisorbed chlorine atoms. Only the configuration with one Cl atom bonded to a Si surface atom is thermally stable up to about 400 °C. The magnitude of the surface core-level shift (930 meV) is smaller than for fluorine on Si(111) [1080 MeV

(Ref. 27)]. This trend is in agreement with first-principles cluster calculations for the two systems¹⁹ which give 1090 (1200) meV for chlorine (fluorine) on Si(111). The existence of three different bonding geometries at room temperature explains the differences² of angle-integrated valence-band photoelectron spectra for adsorption on Si(111)-(7×7) and Si(111)-(2×1). Chlorine on Si(111)-(2×1) has a single geometry contrary to Cl on Si(111)-(7×7) which has multiple-bond geometries at room temperature.

B. Symmetry and dispersion of chlorine-induced bands

The investigation of surface core-level shifts has shown that annealing the chlorine saturated Si(111)-(7×7) surface produces an ordered overlayer of Cl atoms bonded to the silicon substrate atoms in one configuration only. With polarization-dependent angle-resolved photoelectron spectroscopy we now determine the electronic structure of the valence band for this two-dimensional adsorbate system. The polarization dependence of photoemission characterizes the symmetry of the chlorine-induced valence states. Angle-resolved photoelectron spectra allow a mapping of the two-dimensional energy-band structure $E(\mathbf{k}_{\parallel})$. The adsorption geometry and the influence of the interaction with the three-dimensional substrate are determined by comparison with theoretical calculations.

Figure 3 shows the polarization dependence of the intensity of the two main chlorine 3*p*-derived states. The spectra for two different photon energies $\hbar\omega=34$ and 21 eV are shown in an emission direction normal to the surface. In normal emission the final state ($|f\rangle$) of the photoexcitation process is totally symmetric under point-group operations about the surface normal.^{37,38} An initial state ($|i\rangle$) of $\sigma(p_z)$ symmetry is also totally symmetric. A nonvanishing matrix element in dipole approximation ($\langle i | \mathbf{A} \cdot \mathbf{p} | f \rangle$) is, therefore, obtained for an \mathbf{A} vector of the incident light perpendicular to the surface (\mathbf{A}_{\perp}). Photoemission of a $\pi(p_x, p_y)$ state is not allowed for \mathbf{A}_{\perp} but for \mathbf{A} parallel to the surface (\mathbf{A}_{\parallel}). The results of Fig. 3 show that the state with binding energy $E_B=7.95$ eV (below the Fermi energy E_F) has σ symmetry and the one with $E_B=5.2$ eV has π symmetry. The fact that the intensity of the σ state does not completely vanish for \mathbf{A}_{\parallel} can be explained with a not-perfect polarization of the light or with surface umklapp processes from other parts of the surface Brillouin zone (SBZ) due to the (7×7) reconstruction.

TABLE I. Relative energies and intensities of the Si 2*p* bulk and surface contributions.

	Bulk		Surface	
		1^+	2^+	3^+
Intensity after RT adsorption	1	0.42	0.12	0.07
Intensity after annealing	1	0.46		
Core-level shift (relative to bulk)	0 eV	930 meV	1830 meV	2730 meV

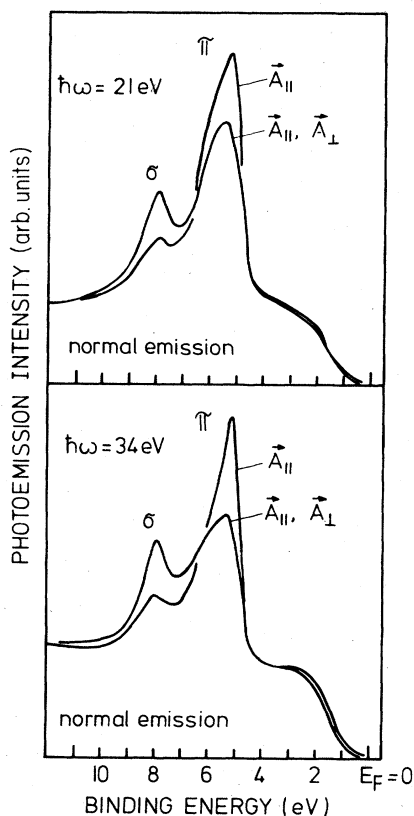


FIG. 3. Normal emission photoelectron spectra for Cl/Si(111)-(7 \times 7) with different polarizations of the incident light (*s* polarized: \vec{A}_{\parallel} ; mixed polarization: \vec{A}_{\parallel} , \vec{A}_{\perp}) and two photon energies ($\hbar\omega=21$ and 34 eV).

The σ state has a 2.75-eV higher binding energy than the π state at the $\bar{\Gamma}$ point of the hexagonal SBZ (see inset of Fig. 4) detected in normal emission. This large energy separation is typical for bonding of chlorine in a onefold site on top of the silicon atoms.^{15,17} For adsorption in a

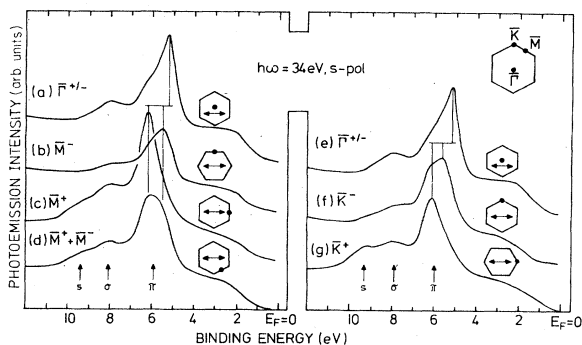


FIG. 4. Angle-resolved photoelectron spectra for emission directions corresponding to different high-symmetry points of the 1 \times 1 surface Brillouin zone (SBZ) for the π states. The symmetry of the detected π state and the relative orientation of the emission (points on the hexagons) and the \vec{A} vector (arrow) are shown for every spectrum.

threefold hollow site σ and π states would be nearly degenerate. The on-top site is also favored by SEXAFS measurements¹¹ and energy-minimization calculations.^{19,20}

The two π states (p_x, p_y) can be classified into states of even and odd parity with respect to the (0 $\bar{1}$ 1) mirror plane. This mirror plane is perpendicular to the surface. The intersection of the two planes is the $\bar{\Gamma}\bar{M}$ direction ($[\bar{2}11]$ in real space). Emission from even π states (π^+) is forbidden for an \vec{A} vector perpendicular to the mirror plane while for odd states (π^-) emission is forbidden for \vec{A} parallel to the mirror plane^{38,39} if the photoelectrons are detected in the mirror plane. Figure 4 shows the results of the application of these selection rules to the chlorine π bands at different points of the 1 \times 1 SBZ. The inset for every spectrum shows the relative orientation of the SBZ, the direction of emission (points) and the orientation of the \vec{A} vector (arrows). All spectra in Fig. 4 are recorded with *s*-polarized light. Figure 4(b) and 4(c) show that at the \bar{M} point the even and odd π states have different binding energy.⁴⁰ At $\bar{\Gamma}$ [see Fig. 4(a)] both states are degenerate for symmetry reasons. Therefore, the dispersion along $\bar{\Gamma}\bar{M}$ is different for the π^+ and π^- band. In Fig. 4(d) a configuration is shown where emission from both the even and odd band is allowed and in fact the broad peak around 6-eV binding energy contains contributions from both bands (π^+, π^-). If only the nearest-neighbor interaction of the chlorine overlayer to the substrate is taken into account the surface has a sixfold rotational symmetry and the plane containing the $\bar{\Gamma}\bar{K}$ direction ($[\bar{1}10]$ in real space) is also a mirror plane. We applied the dipole selection rules also for the \bar{K} points in the reciprocal space. The results are shown in Figs. 4(e)–4(g). For the \bar{K}^+ configuration only one chlorine π state is seen in the spectrum [Fig. 4(f)]. But the spectrum of Fig. 4(g) with \bar{K}^- configuration clearly shows emission out of two states although only the π^- state should be seen if the mirror symmetry was perfect. Thus, the interaction to silicon substrate atoms of the second layer and below has to be considered and the sixfold symmetry reduces to a threefold symmetry. The effect of the full substrate symmetry can, therefore, not be neglected in the interpretation of the spectra as will be seen below in the interpretation of the band dispersion. Beside the σ and π band Fig. 4 also shows another structure in the photoemission spectra around 9.5-eV binding energy denoted with *s*. While the σ state is a bonding Cl(p_z)-Si(p_z) state the *s* state is characterized as a bonding Cl(p_z)-Si(*s*) state.⁷ The results of the band dispersion and the angular distribution of photoemission shown later confirm this assignment.

The two-dimensional dispersion $E(\mathbf{k}_{\parallel})$ can be mapped directly with angle-resolved spectra whereby the polar angle θ and the azimuth ϕ fix \mathbf{k}_{\parallel} . The magnitude of \mathbf{k}_{\parallel} is obtained with the kinetic energy (E_{kin}) of the photoelectrons and the polar angle of emission via $k_{\parallel} = (2m_e)^{1/2}\hbar^{-1}(E_{\text{kin}})^{1/2}\sin\theta$. Figure 5 shows two selected scans of angle-resolved spectra along the high-symmetry direction $\bar{\Gamma}\bar{M}\bar{\Gamma}$ and $\bar{\Gamma}\bar{K}\bar{M}$ of the SBZ (see inset of Fig. 6). The chosen polarization of the light allows photoemission from even π states only. The spectra show the dispersionless *s* and σ states. The π band disperses down-

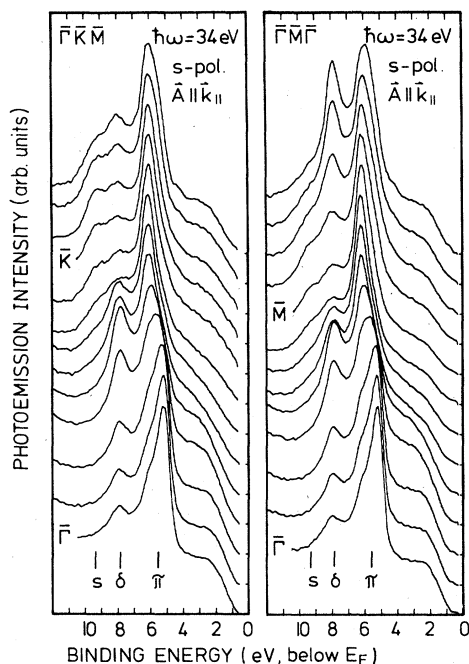


FIG. 5. Angle-resolved photoelectron spectra for the azimuthal directions $\Gamma\bar{K}\bar{M}$ (left panel) and $\Gamma\bar{M}\bar{\Gamma}$ (right panel). The spectra (original data) are plotted with polar angle changes of $\Delta\theta=3^\circ$.

ward from $\bar{\Gamma}$ to \bar{M} and \bar{K} . Figure 6 summarizes the experimental data for the band dispersion. To compare the experimental results with band-structure calculations the binding energy has to be referred to the valence-band

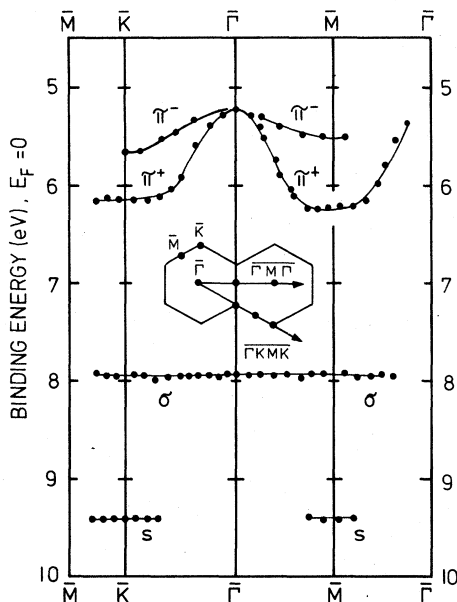


FIG. 6. Experimental band dispersion of the chlorine-induced states for Cl/Si(111)-(7 \times 7).

TABLE II. Energies of critical points of the chlorine-induced bands measured relative to the valence-band maximum with an uncertainty of ± 0.05 eV. Energy in eV.

	$\bar{\Gamma}$	\bar{M}	\bar{K}
π^-	4.46	4.78	4.91
π^+	4.46	5.46	5.36
σ	7.21	7.21	7.21
s	8.7	8.7	8.7

maximum (E_V) and not to the Fermi energy (E_F). For the clean Si(111)-(7 \times 7) surface the difference $E_F - E_V$ is 630 meV.⁴¹ The change of the band bending with chlorine adsorption can be measured with the shift of the Si 2*p* bulk core-level energy. This measurement has been carried out with a photon energy of $\hbar\omega=110$ eV in a bulk sensitive mode and yields a band-bending change of 110 meV. For Cl/Si(111)-(7 \times 7) we get, therefore, $E_F - E_V = 740$ meV. The experimental critical points of the chlorine energy bands are listed in Table II with the valence-band maximum E_V as reference energy.

In Fig. 7 our experimental results (upper-left panel) are compared with the results of a self-consistent pseudopotential calculation carried out by Schlüter *et al.*^{7,13} for the adsorption of Cl on an ideal Si(111)-(1 \times 1) surface (upper-right panel). The lower panel of Fig. 7 shows the bands of a free chlorine monolayer calculated with the LCAO method by Batra and Chen¹⁶ to demonstrate the effect of the Cl-Cl interaction on the surface-energy bands. The monolayer shows only one p_z -band. Upon interaction with the substrate this band splits into two bonding Cl(p_z)-induced bands, namely σ [Cl(p_z)-Si(p_z)] and s [Cl(p_z)-Si(s)]. Both bands are observed in the photoemission experiment although their binding energy is too large in theory compared to the experiment. As a consequence,

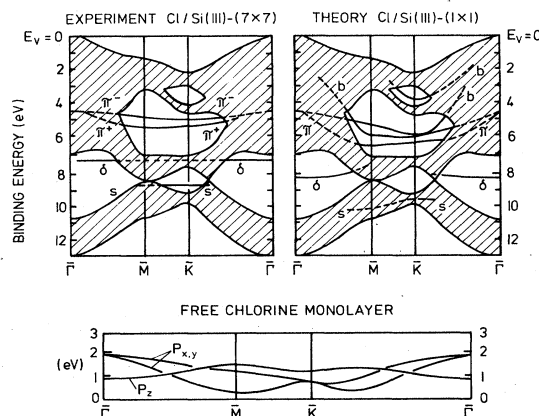


FIG. 7. Comparison of experimental and theoretical surface energy bands: experimental results for Cl/Si(111)-(7 \times 7) (upper-left panel), theoretical results of a self-consistent pseudopotential calculation for Cl/Si(111)-(1 \times 1) after Ref. 7 (upper-right panel), and an LCAO calculation for a free-chlorine monolayer after Ref. 16 (lower panel).

the s state lies in a gap of the projected silicon band structure (dashed areas) around the \bar{K} point and overlaps with bulk band around \bar{M} . This behavior is similar to the results for Cl/Si(111)-(2 \times 1).⁷ The calculation, however, predicts that the s -state overlap the projected Si band both at \bar{M} and \bar{K} .

The effect of the interaction with the substrate onto the dispersion the bands is clearly seen at the \bar{K} point. Here the two bands are degenerate for symmetry reasons for the

free chlorine monolayer. The observed splitting of 450 meV is an effect of the interaction with the substrate which also leads to a breaking of the mirror-plane selection rule for $\bar{\Gamma}\bar{K}$ as discussed before. If the surface is no longer sixfold symmetric but only threefold, the six equivalent \bar{M} points split into two sets of three equivalent ones (\bar{M}, \bar{M}'). For two-dimensional states the band energies at \bar{M} and \bar{M}' are still degenerate because of time-reversal symmetry. The observed dispersion of is the

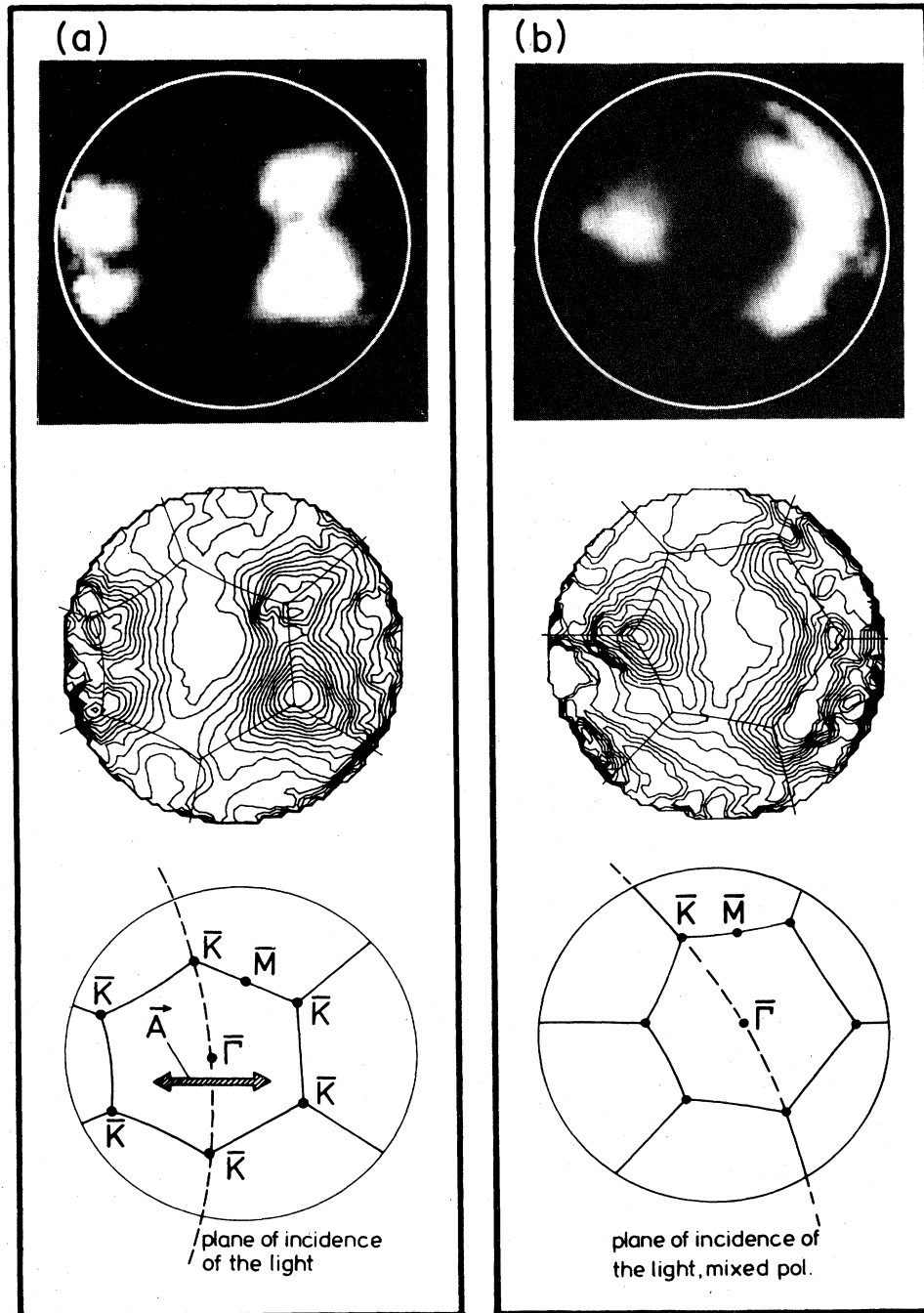


FIG. 8. Angular distribution pictures of photoemission out of the chlorine s state as intensity pictures and as contour map together with a projection of the surface Brillouin zone for two different polarizations [(a) s polarization (b) mixed sp polarization].

same for $\bar{\Gamma}\bar{M}$ and $\bar{\Gamma}\bar{M}'$ because at \bar{M},\bar{M}' the π states are true two-dimensional surface states and do not overlap with substrate bands (see Fig. 7). The theoretical results predict a further type of chlorine-induced surface states (b) associated with the modification of the back-bonding orbitals between the first and second silicon layer upon adsorption.⁷ An evidence of such structures has not been found in our photoelectron spectra. Between $E_V + 1$ eV and $E_V + 4$ eV we only see a broad structureless reso-

nance after chlorine adsorption.

The results above show that the dispersion of the chlorine bands can be successfully described with a SBZ of (1×1) symmetry. This supports a structure with the existence of large areas of ideal (1×1) surface structure. It has been shown that a checkerboard pattern of triangular areas with 1×1 structure gives rise to starlike LEED patterns similar to the " (7×1) " structure.³⁵ Several models of the types proposed^{35,36} can explain the observed

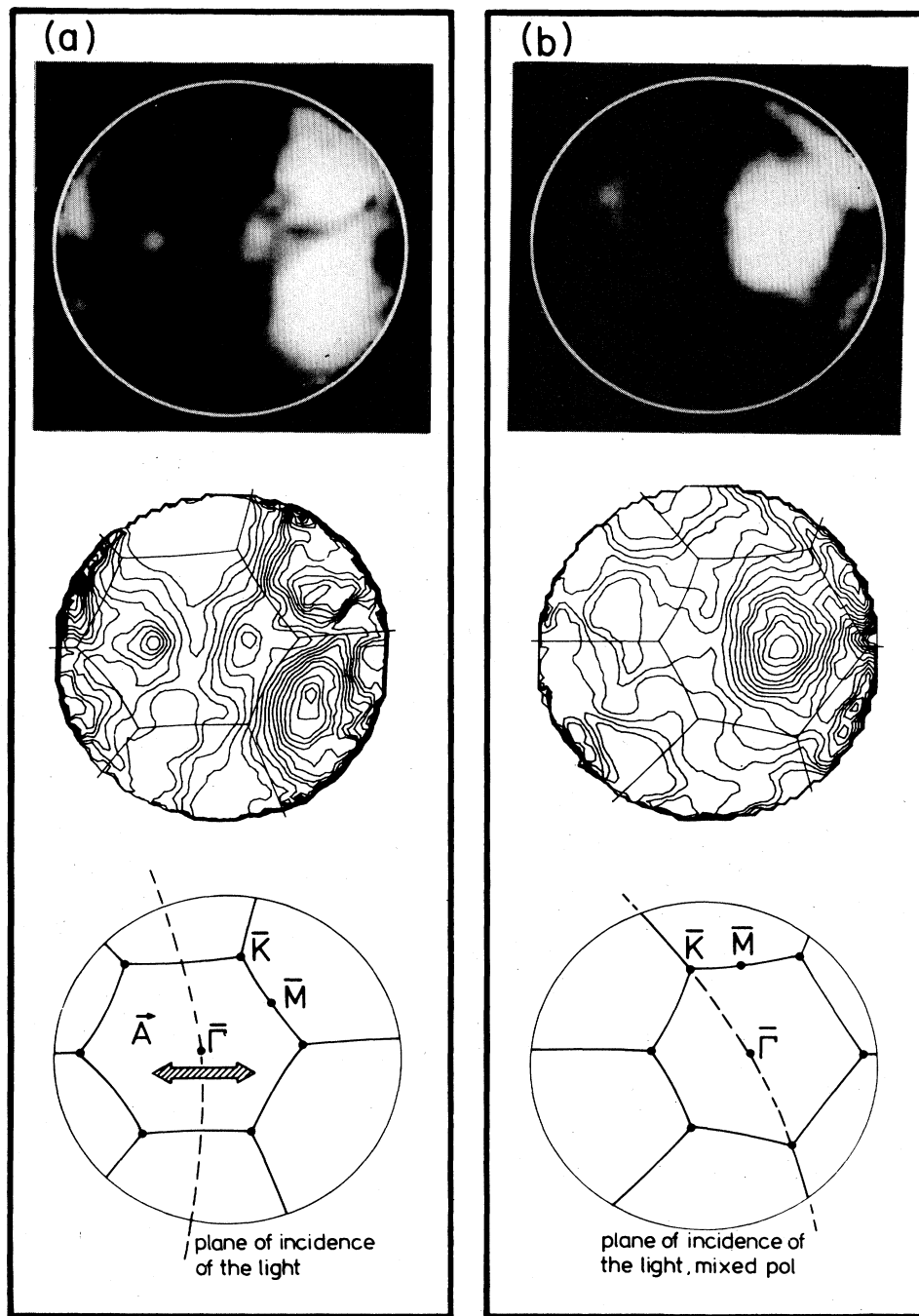


FIG. 9. Angular distribution pictures of photoemission out of the chlorine σ state as intensity picture and as contour map together with a projection of the surface Brillouin zone for two different polarizations [(a) s polarization, (b) mixed sp polarization].

LEED pattern as well as the core-level data and the (1×1) dispersion. With these models one has differently stacked areas with ideal (1×1) structure with chlorine atoms on top of every silicon surface atom. The boundaries of these areas have a structure similar to the clean Si(111)-(7 \times 7) surface.³⁴

C. Photoemission angular distribution

The angular distribution of photoelectrons emitted from an atom or molecule chemisorbed on a surface contains information about the character of the orbitals involved and the geometry of the surface complex.⁴² A realistic calculation of photoemission intensities needs the knowledge of the initial- and final-state wave functions and the microscopic behavior of the electromagnetic field vector (\mathbf{A}) in the surface.^{38,43} Photoemission intensities have been mostly interpreted and calculated in terms of localized adsorbate orbitals or surface clusters of limited size. But for a full monolayer coverage one has a lateral interaction of the adsorbed atoms that results in the formation of the two-dimensional energy bands. This surface band character of the initial state of the photoexcitation process influences the angular intensity profile.^{44,45} We have examined the angular distribution of photoemission out of the bonding σ and s levels and see structures that can be related to the hybridization of the two-dimensional adsorbate states with the three-dimensional band structure of the substrate.

Already in Fig. 5 polar angle variations of the σ and s photoemission intensities can be seen. Figures 8 and 9 show two-dimensional angular distribution pictures (ADP's) of photoemission out of these states for $\hbar\omega = 34$ eV within the acceptance cone of about 88° (for a description of the data evaluation see Ref. 42). The intensities of both states were strongest in this photon energy range. The intensity distribution on the phosphor screen behind the microchannel plates is displayed as a direct image of the video screen (bright spots correspond to high intensity) and as a contour map. A projection of the SBZ via the projection k_{\parallel} of the photoelectron momentum \mathbf{k} is shown together with every ADP. Two different sample positions and, hence, two different polarizations of the light are chosen (s polarization in Figs. 8(a) and 9(a), and mixed sp polarization in Figs. 8(b) and 9(b)). The ADP's are recorded for fixed kinetic energies corresponding to the maximum emission of the two states. As both states are non-dispersive the ADP's are not influenced by k_{\parallel} dispersion effects.⁴⁴ As seen in Fig. 8(a) intensity maxima for the s state are seen at the zone boundary especially at four of the six \bar{K} points. In the plane of incidence no emission is detected. The ADP's have been measured with a fixed orientation of the sample relative to the incident light. Therefore, the scalar product $\mathbf{A} \cdot \mathbf{p}$ in the dipole matrix element changes for every emission direction and the ADP's are strongly influenced by polarization effects. In a configuration with s -polarized light as in Figs. 8(a) and

9(a) emission in the plane of incidence is forbidden for $\sigma(s)$ states due to dipole selection rules (see above). As a consequence emission at the two \bar{K} points in the plane of incidence is suppressed in Fig. 8(a). Figure 8(b) shows that for a different azimuthal orientation of the sample and for different light polarization the strongest photoemission is still seen at \bar{K} points.

The ADP of photoemission out of the σ state behaves in a very different way. Here emission is attenuated at the zone boundary and maxima are seen in the middle of the SBZ's in the repeated zone scheme. In Fig. 9(a) again emission in the plane of incidence and especially at $\bar{\Gamma}$ is forbidden. With mixed polarization [Fig. 9(b)], however, a maximum is also seen in the center of the first SBZ because emission is no longer forbidden. In summary, the structures of the ADP's can be correlated to the SBZ. The σ state is most intense in the center of the SBZ and the s state at the zone boundary at the \bar{K} points unless dipole selection rules do not allow emission. Looking at the chlorine surface band structure and the projected silicon bulk band structure in Fig. 7 these observations can be generalized. Photoemission out of these two states is most intense in parts of the SBZ where they exist as true surface states without overlapping to the silicon bands and is attenuated where they exist as surface resonances overlapping the projected silicon band structure. As surface resonances the chlorine bands hybridizes with silicon bands of proper symmetry. Calculations by Liebsch⁴⁴ predicted a significant broadening of the adsorbate levels of ordered oxygen and sulphur layers on Ni(100) caused by the hybridization with the three-dimensional substrate bands. Recently, first evidence of such momentum-dependent hybridization has been observed.⁴⁶ This broadening is accompanied by a reduction of the maximum peak height measured in our case which can explain the angular intensity distribution observed in the ADP's. The spectra in Fig. 5 illustrate that the chlorine-induced structures are typically 1–1.5 eV broad at full width at half maximum (FWHM) and that the slopes of the structures overlap. As a consequence a change of the peak width for different emission directions cannot be detected unambiguously. The above results show that an interpretation in a purely localized orbital approach for the σ and s state is not sufficient to describe the photoemission intensities. A correlation between the ADP's and the SBZ has been found. Their character as extended two-dimensional states has to be taken into account. Further theoretical work is necessary to give a more detailed interpretation.

ACKNOWLEDGMENTS

We would like to thank the staff of BESSY, Berlin, and especially W. Braun for support. We further acknowledge the help of B. Konrad and Th. Weser. This work has been supported by the Bundesministerium für Forschung und Technologie from funds for synchrotron radiation research.

- *Permanent address: IBM Thomas J. Watson Research Center, Yorktown Heights, New York 10598.
- †Permanent address: Institut für Physikalische Chemie der Universität München, D-8000 München 2, Federal Republic of Germany.
- ¹G. Margaritondo, J. E. Rowe, C. M. Bertoni, C. Calandra, and F. Manghi, *Phys. Rev. B* **20**, 1538 (1979).
 - ²J. E. Rowe, G. Margaritondo and S. B. Christman, *Phys. Rev. B* **16**, 1581 (1977).
 - ³For a review of earlier results see H. H. Farrell, in *The Chemical Physics of Solid Surfaces and Heterogeneous Catalysis*, edited by D. A. King and D. P. Woodruff (Elsevier, Amsterdam, 1984), Vol. 3B, Chap. 5.
 - ⁴J. E. Rowe, *Surf. Sci.* **53**, 461 (1975); *J. Vac. Sci. Technol.* **12**, 293 (1975).
 - ⁵M. Schlüter, J. E. Rowe, G. Margaritondo, K. M. Ho, and M. L. Cohen, *Phys. Rev. Lett.* **37**, 1632 (1976).
 - ⁶K. C. Pandey, T. Sakurai, and H. D. Hagstrum, *Phys. Rev. B* **16**, 3648 (1977).
 - ⁷P. K. Larsen, N. V. Smith, M. Schlüter, H. H. Farrell, K. M. Ho, and M. L. Cohen, *Phys. Rev. B* **17**, 2612 (1978).
 - ⁸P. E. Best, *Phys. Rev. B* **19**, 1054 (1979).
 - ⁹M. Schlüter, J. E. Rowe, S. P. Weeks, and S. B. Christman, *J. Vac. Sci. Technol.* **16**, 615 (1979).
 - ¹⁰K. Fujiwara, *Solid State Commun.* **36**, 241 (1980).
 - ¹¹P. H. Citrin, J. E. Rowe, and P. Eisenberger, *Phys. Rev. B* **28**, 2299 (1983); P. H. Citrin and J. E. Rowe, *Surf. Sci.* **132**, 205 (1983); P. H. Citrin, J. E. Rowe, P. Eisenberger, and F. Comin, *Physica (Utrecht)* **117B/118B**, 786 (1983).
 - ¹²M. Nishida, N. Ishii, and T. Shimizu, *Phys. Lett.* **60A**, 148 (1977).
 - ¹³M. Schlüter and M. L. Cohen, *Phys. Rev. B* **17**, 716 (1978).
 - ¹⁴K. Mednick and C. C. Lin, *Phys. Rev. B* **17**, 4807 (1978).
 - ¹⁵K. Mednick and C. C. Lin, *Surf. Sci.* **81**, 347 (1979).
 - ¹⁶I. P. Batra, *J. Vac. Sci. Technol.* **16**, 1359 (1979), M. Chen and I. P. Batra, *ibid.* **16**, 570 (1979).
 - ¹⁷K. Zhang and L. Yeh, *J. Vac. Sci. Technol.* **19**, 628 (1981).
 - ¹⁸T. Hoshino and M. Tsukada, *Surf. Sci.* **115**, 104 (1982).
 - ¹⁹M. Seel and P. S. Bagus, *Phys. Rev. B* **18**, 2023 (1983); M. Seel (private communication).
 - ²⁰G. B. Bachelet and M. Schlüter, *Phys. Rev. B* **28**, 2302 (1983); G. B. Bachelet and M. Schlüter, *J. Vac. Sci. Technol. B* **1**, 726 (1983).
 - ²¹N. F. Winters, J. W. Coburn, and T. J. Chuang, *J. Vac. Sci. Technol. B* **1**, 469 (1983).
 - ²²W. Braun and J. Jäkisch, *Proceedings of the 7th International Conference on Vacuum Ultraviolet Radiation Physics* [*Ann. Isr. Phys. Soc.* **6**, 182 (1983)].
 - ²³D. Rieger, R. D. Schnell, W. Steinmann, and V. Saile, *Nucl. Instrum. Methods* **208**, 777 (1983).
 - ²⁴R. D. Schnell, D. Rieger, and W. Steinmann, *J. Phys. E* **17**, 221 (1984).
 - ²⁵R. D. Schnell, D. Rieger, A. Bogen, K. Wandelt, and W. Steinmann, *Solid State Commun.* **53**, 205 (1985).
 - ²⁶D. Menzel in *Photoemission and the Electronic Properties of Surfaces*, edited by B. Feuerbacher, B. Fitton, and R. F. Willis (Wiley, New York, 1978), Chap. 13.
 - ²⁷G. Hollinger and F. J. Himpsel, *Phys. Rev. B* **28**, 3651 (1983); *Appl. Phys. Lett.* **44**, 93 (1984).
 - ²⁸F. R. McFeely, J. F. Morar, N. D. Shinn, G. Landgren, and F. J. Himpsel, *Phys. Rev. B* **30**, 764 (1984); J. F. Morar, F. R. McFeely, N. D. Shinn, G. Landgren, and F. J. Himpsel, *Appl. Phys. Lett.* **45**, 175 (1984).
 - ²⁹F. R. McFeely, J. F. Morar, and F. J. Himpsel, *Surf. Sci.* (to be published).
 - ³⁰T. J. Chuang, *J. Appl. Phys.* **51**, 2614 (1980).
 - ³¹S. C. McNamin and G. E. Becker, *J. Vac. Sci. Technol. B* **3**, 485 (1985).
 - ³²D. J. Ehrlich, R. M. Osgood, and T. F. Deutsch, *Appl. Phys. Lett.* **38**, 1018 (1981).
 - ³³G. Binnig, H. Rohrer, Ch. Gerber, and E. Weibel, *Phys. Rev. Lett.* **50**, 120 (1983).
 - ³⁴For a discussion of proposed structural models see, e.g., R. M. Tromp and E. J. van Loenen, *Surf. Sci.* **155**, 441 (1985).
 - ³⁵Himpsel, *Phys. Rev. B* **27**, 7782 (1983); F. J. Himpsel and I. P. Batra, *J. Vac. Sci. Technol. A* **2**, 952 (1984).
 - ³⁶E. G. McRae and C. W. Caldwell, *Phys. Rev. Lett.* **46**, 1632 (1981); E. G. McRae, *Surf. Sci.* **124**, 106 (1983); **147**, 663 (1984).
 - ³⁷W. Eberhardt, G. Kalkoffen, C. Kunz, D. Aspnes, and M. Cardona, *Phys. Status Solidi* **88**, 135 (1978).
 - ³⁸For a review of angle-resolved photoemission see, e.g., E. W. Plummer and W. Eberhardt, *Adv. Chem. Phys.* **49**, 533 (1982); F. J. Himpsel, *Adv. Phys.* **32**, 1 (1983).
 - ³⁹J. Hermanson, *Solid State Commun.* **22**, 9 (1977).
 - ⁴⁰In previous angle-resolved experiments (Ref. 7) the geometry was such that only the π^+ band could be detected.
 - ⁴¹F. J. Himpsel, G. Hollinger, and R. A. Pollack, *Phys. Rev. B* **28**, 7014 (1983).
 - ⁴²D. Rieger, R. D. Schnell, and W. Steinmann, *Surf. Sci.* **143**, 157 (1984).
 - ⁴³For a review of the theory of photoemission from adsorbates see, e.g., G. Doyen and T. B. Grimley in Ref. 26, Chap. 6; A. Liebsch, in Ref. 26, Chap. 7; A. Schichl, Ph.D thesis, Technische Universität München, 1980.
 - ⁴⁴A. Liebsch, *Phys. Rev. Lett.* **38**, 248 (1977); A. Liebsch, *Phys. Rev. B* **17**, 1653 (1978); E. W. Plummer, B. Tonner, N. Holzwarth, and A. Liebsch, *ibid.* **21**, 4306 (1980).
 - ⁴⁵J. W. Gadzuk, *Surf. Sci.* **53**, 132 (1975).
 - ⁴⁶R. A. DiDio, E. W. Plummer, and W. R. Graham, *Phys. Rev. Lett.* **52**, 683 (1984).

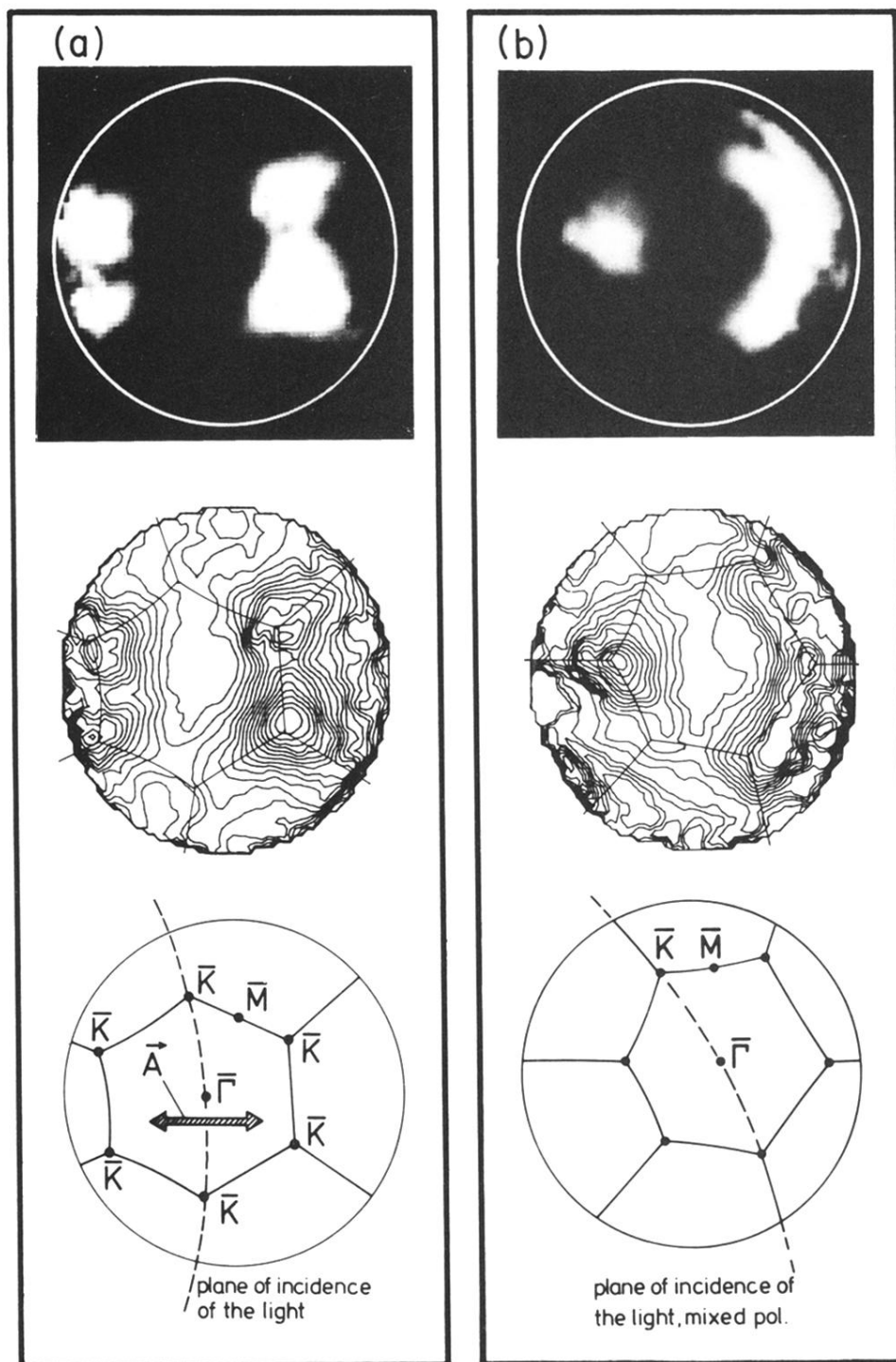


FIG. 8. Angular distribution pictures of photoemission out of the chlorine s state as intensity pictures and as contour map together with a projection of the surface Brillouin zone for two different polarizations [(a) s polarization (b) mixed sp polarization].

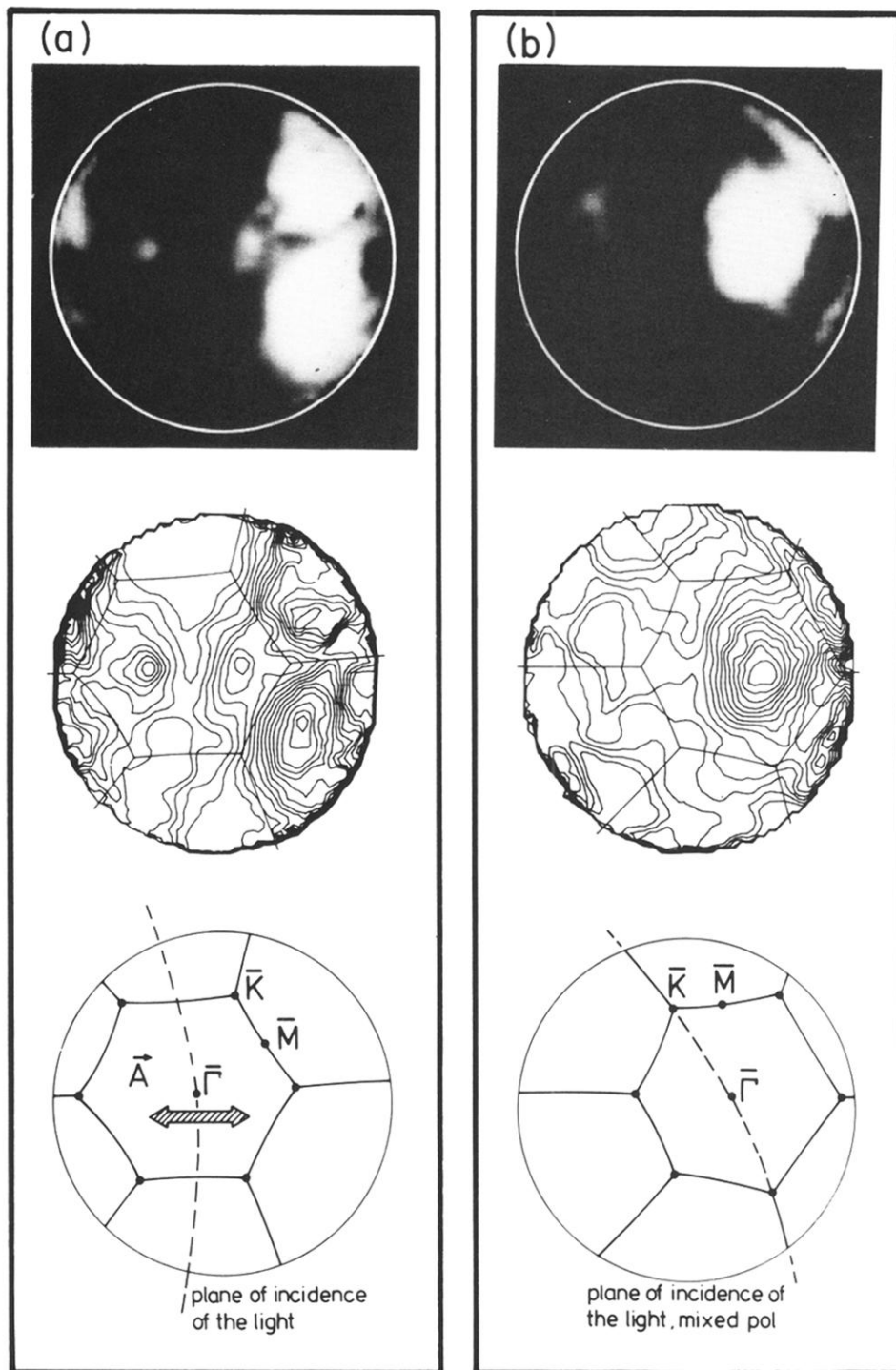


FIG. 9. Angular distribution pictures of photoemission out of the chlorine σ state as intensity picture and as contour map together with a projection of the surface Brillouin zone for two different polarizations [(a) s polarization, (b) mixed sp polarization].